# Standoff Detection of Thermal and Fast Neutrons

Anthony L. Hutcheson, Bernard F. Phlips, Eric A. Wulf, Lee J. Mitchell, Richard S. Woolf
Radiation Detection Section (Code 7654)
High Energy Space Environment Branch
U.S. Naval Research Laboratory
Washington, DC, USA

***Abstract*—Improved detection of weapons of mass destruction is one of the Science and Technology priorities of the Secretary of Defense for Fiscal Years 2013-2017. Unfortunately, the remote detection of special nuclear materials is difficult because the materials are not very radioactive, the radiation signatures decrease rapidly with distance, and faint sources of radiation can be obscured by naturally occurring and man-made radioactive sources. The Radiation Detection Section of the High Energy Space Environment Branch of the U.S. Naval Research Laboratory has developed a containerized fast and thermal neutron standoff detection system. The instrument was characterized with neutron sources at different standoff distances and at different drive-by speeds to determine the on-water performance of the system. Results of this measurement campaign will be discussed.**

***Keywords-standoff detection; mobile detection; neutron detection; special nuclear materials***

## I. INTRODUCTION

Leveraging a heritage of developing large scale, mobile systems for the detection and localization of radioactive materials [1-3], the Radiation Detection Section of the High Energy Space Environment Branch of the U.S. Naval Research Laboratory (NRL) has developed a containerized system for the standoff detection of both thermal and fast neutrons. The characterization of this large array, both stationary and in motion, will help in the understanding of the capabilities and limits of passive neutron detection both on land and at sea.

## II. SYSTEM DESCRIPTION

The neutron detection system is housed within a 20-ft refrigerated ISO container (see Figure 1) that provides temperature and humidity control. Power for the system is provided by a clip-on diesel generator capable of providing approximately 5 days of continuous operation. In addition, the system is equipped with a pair of global positioning system (GPS) receivers to determine location, speed, and orientation. On-board electronics are additionally protected from power fluctuations by a rack-mounted UPS and can be accessed and controlled via an external Ethernet port on the front of the ISO container.

The neutron detection system comprises two separate subsystems for the detection of thermal and fast neutrons. A

**Figure 1: Photo of the containerized detection system.**

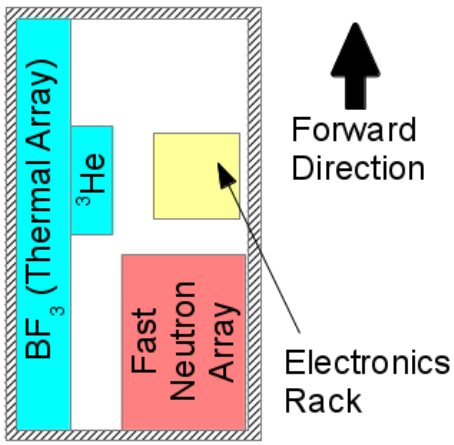


**Figure 2: Sketch of the layout of the containerized system.**

general layout of the total system is shown schematically in Figure 2. The thermal neutron subsystem is located on the port side of the container and spans the entire container wall on that side; the fast neutron system is located on the aft starboard side of the container near the electronics rack. The specific details of each of these two subsystems will be addressed in the following subsections.

### *A. Thermal Neutron Detection*

The thermal neutron subsystem comprises 24 $BF_3$ (Ø11.4 × 183 cm; 93.2 kPa) (LND, Inc., Oceanside, NY, USA) and six GE Reuter Stokes $^3$He detectors (Ø14.7 × 64.0 cm; 270 kPa).

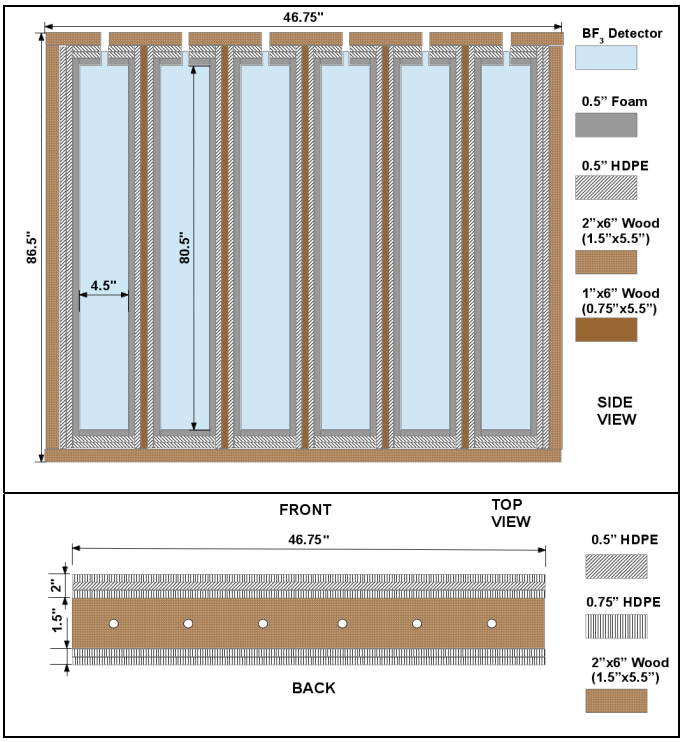


**Figure 3: Sketch of the $BF_3$ modules.**


**Figure 4: Photo of one of the EJ-309 liquid scintillator detectors.**

The $BF_3$ array is composed of four modules of six detectors surrounded by at least 2.5 cm of high density polyethylene (HDPE) on all sides; a schematic of the modular structures is shown in Figure 3. High voltage is applied and pulse signals

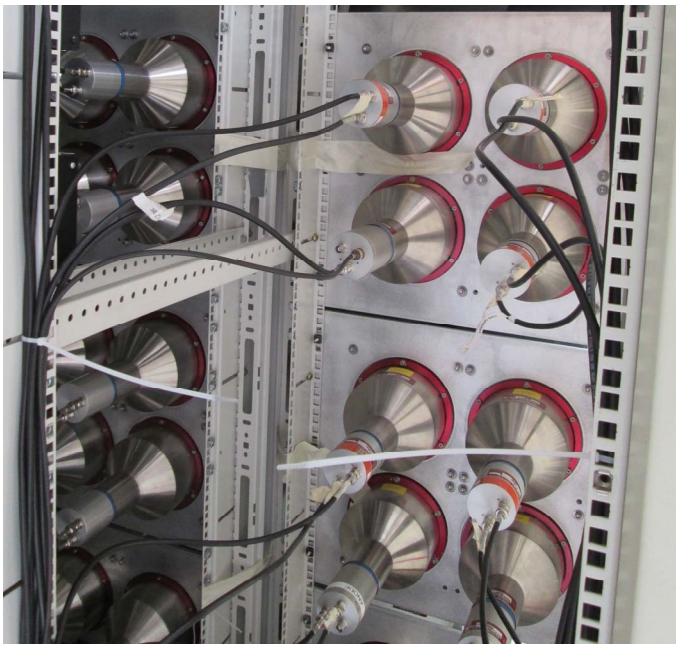

**Figure 5: Photograph of a portion of the fast neutron detection array from the rear.**

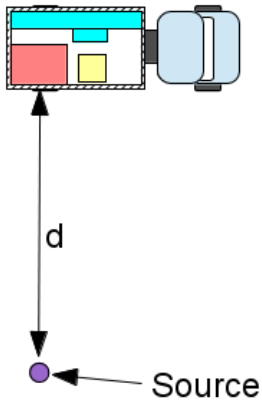


**Figure 6: Setup of stationary measurements.**

obtained from the single SHV input/output of each $BF_3$ detector via ORTEC 142AH preamplifiers (ORTEC, Oak Ridge, TN, USA); the output pulses from the preamps are input into Mesytec MSCF-16 shaping amplifiers (Mesytec GmbH & Co. KG, Putzbrunn, Germany) followed by a Mesytec MADC-32 peak sensing ADC. The ADC data buffers are time tagged with the system clock of the readout computer, which is synchronized with the onboard GPS system using the Network Time Protocol (NTP). To provide accurate time stamps for each event, each ADC is provided a 10-MHz external oscillator signal from a Stanford Research Systems FS725 rubidium oscillator, which in turn is trained to the pulse-per-second (PPS) signal from the onboard GPS module.

The $^3$He array is housed in a smaller module composed entirely of 2.5-cm-thick HDPE. These detectors each provide

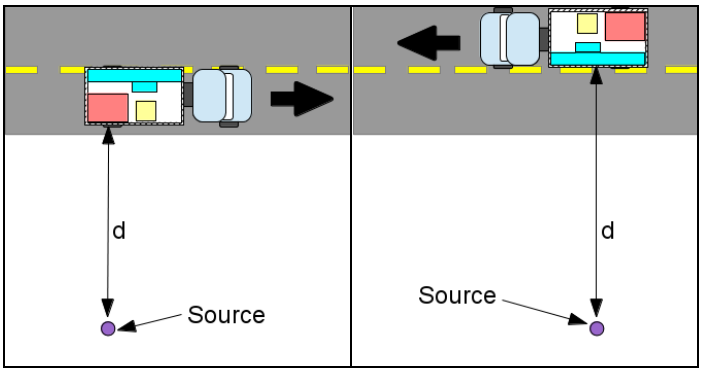


**Figure 7: Sketch of the mobile neutron measurements. (left) Fast system bias. (right) Thermal system bias.**

two outputs: a TTL trigger signal and a Gaussian-shaped amplitude signal that was input directly into a Mesytec MADC-32.

### *B. Fast Neutron Detection*

The fast neutron detection subsystem comprises a 6 × 8 array of EJ-309 liquid scintillator detectors (15.2 × 15.2 × 15.2 cm) coupled to ETL 9390KB photomultiplier tubes (PMTs); the detector pitch of the array is 18.4 cm. A photograph of one of the liquid scintillator detectors is shown in Figure 4; a photograph of a portion of the array from the rear is shown in Figure 5. HDPE neutron shielding was placed above and below (7.6 cm thickness) as well as to the right (8.9 cm thickness) of the array; the left side of the array was left unshielded due to electronics access and cabling. The output signals from each PMT are processed via Struck SIS3316 16-channel VME flash ADCs (Struck Innovative Systeme GmbH, Hamburg, Germany). These 14-bit modules have a 250-MHz sampling rate and allow the user to utilize pulse shape discrimination (PSD) techniques to separate fast neutron events from those produced by incident gammas. Pulse height thresholds and gains were adjusted to provide a dynamic range of neutron energies from approximately 900 keV to 6.0 MeV. Four flash ADCs are necessary to handle all 48 detectors as well as a PPS signal from the onboard GPS module. The ADCs share a 250-MHz clock that is generated on the master SIS3316 board from the GPS-trained 10-MHz rubidium oscillator and distributed to the remaining three modules. These time markers provide a way to correlate the timing of the flash ADC system to that of the Mesytec MADC system used for the thermal detection system as well as to the slow-logged, peripheral data such as onboard temperature and GPS coordinates.

## III. METHODS

To characterize the neutron detection capabilities of each subsystem, a $^{252}$Cf source (8.3 MBq; reference date 18 Nov 2013) was used to provide fission-spectrum neutrons. At the time of the measurements reported herein (Sep 2014), the source produced approximately 775,000 neutrons/s. The performance of the system was characterized in both stationary and mobile operations.

### *A. Stationary Measurements*

Stationary measurements were performed in a large, mostly empty on-site parking lot at NRL. As shown in Figure 6, the $^{252}$Cf was positioned on the starboard side of the container at various standoff distances ranging from approximately 7.0 to 122.0 m; the starboard side was chosen in deference to the increased directional sensitivity of the fast neutron array compared to the thermal neutron array. Each source position was measured with an Adafruit Ultimate GPS unit connected to a BeagleBone Black low-power single-board computer. These source coordinates were compared to the GPS coordinates recorded on the system container to calculate accurate standoff distances.

### *B. Mobile Measurements*

Following the stationary measurements, further measurements were performed with the neutron detection system in motion. The $^{252}$Cf was positioned at various standoff distances from an on-site road at NRL, and the neutron system was driven by at speeds of approximately 2.2, 4.4, and 8.9 m/s. The source was positioned either atop a 2.5-m ladder or at the top of a portable 5-m aluminum mast to provide a clear view to the system above both stationary and mobile obstructions. As for the stationary measurements, the portable GPS unit was used to determine the coordinates of the source location, which were compared to the GPS coordinates of the mobile container to determine the standoff distance of closest approach for the system. Two sets of mobile measurements were taken: one with the source on the starboard (fast neutron array) side, and one on the port (thermal neutron array) side. Standoff distances ranged up to approximately 120 m. Sketches of the basic concept of these mobile measurements are shown in Figure **7**.

## IV. RESULTS

### *A. Thermal Neutron Detection*

During the course of the measurements described in this work, one of the preamps for the 24 $BF_3$ detectors suffered a failure; as a result, only the pulses from the remaining 23 $BF_3$ detectors as well as the six $^3$He detectors were used in the analysis. The background neutron count rate of 37.0 counts/s was calculated from over 12 h of data, including time before, after, and between neutron source measurements.

The average count rates measured for approximately 5 minutes of acquisition at various stationary standoff distances are given in Figure 8. The error bars shown represent the actual measured standard deviation of the counts over the integration period. Based on the measured background rate and a 3σ detection level, the thermal detection system would alarm on this source with a 1-s integration at standoff distances of up to 60 m; for a 5-s integration, the system would alarm for standoff distances up to approximately 100 m.

For mobile detections, depending on the drive-by speed and the standoff distance to the source, the detection system may only have a viable integration window of a few seconds. A representative example of the count rate for a drive-by pass (55 m closest approach, 2.6 m/s) is shown in Figure 9. As such,

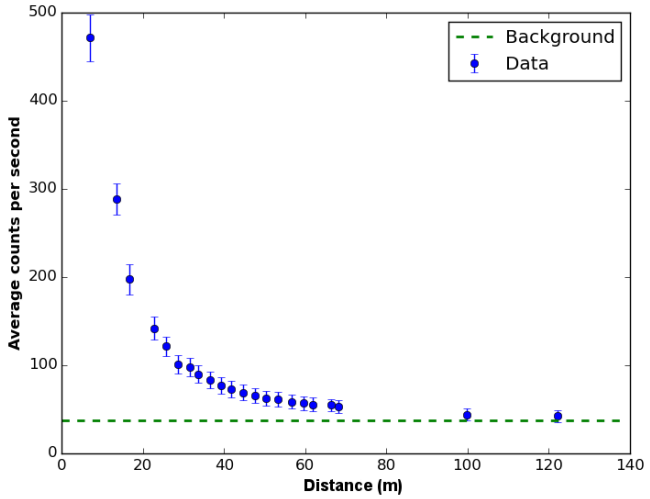


**Figure 8: Average neutron counts per second measured by the thermal detection system for stationary measurements. Averages represent approximately 5 min of integration time; error bars represent the actual standard deviations of the data over this integration time.**

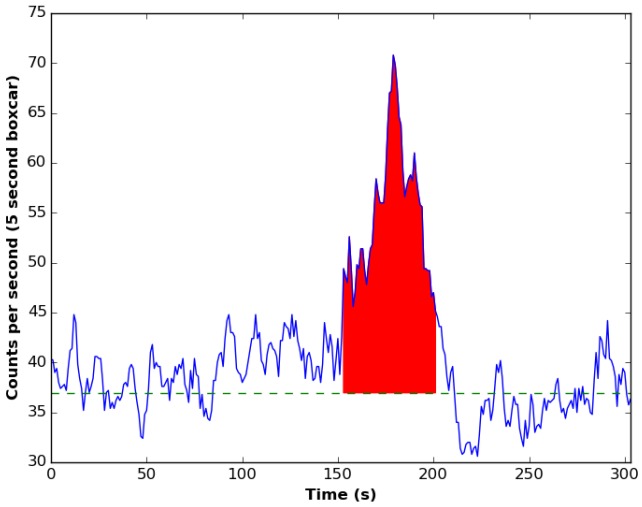


**Figure 9: Representative rate plot for drive-by detection of neutron source (55 m closest approach, 2.6 m/s). The red area indicates the period during which the count rate was greater than 3σ above background.**

based on the results of the standoff measurements, the system may be predicted to struggle to alarm for drive-by closest approaches of approximately 100 m or greater. The detection results for the thermal neutron detection system are given in Table 1. For each run, a moving boxcar average of counts was used to determine if the system alarmed on the source; to maintain a symmetric window about the current second, only odd integer window lengths (e.g., 1, 3, and 5 s) were chosen. The minimum boxcar window length, if any, at which the system alarmed above a 3σ level is given for each run. Note

**Table 1: Results for mobile detection of neutron source by thermal neutron system.**

| Distance (m) | Speed (m/s) | Detection (Y/N) | Boxcar (s) |
|---|---|---|---|
| 55 | 2.8 | Y | 1 |
| 55 | 2.9 | Y | 1 |
| 55 | 2.6 | Y | 1 |
| 55 | 2.6 | Y | 1 |
| 55 | 2.7 | Y | 1 |
| 65 | 2.5 | Y | 1 |
| 65 | 2.6 | Y | 1 |
| 65 | 4.5 | Y | 3 |
| 65 | 4.3 | Y | 1 |
| 75 | 2.5 | Y | 3 |
| 75 | 2.5 | Y | 3 |
| 75 | 4.6 | Y | 3 |
| 75 | 4.9 | Y | 5 |
| 90 | 2.7 | Y | 3 |
| 90 | 2.7 | Y | 5 |
| 120.0 | 2.2 | N | --- |
| 120.0 | 2.2 | N | --- |

that, as expected, the system successfully alarmed for closest approaches of approximately 90 m at drive-by speeds of approximately 4.4 m/s but failed to alarm at the greater measured standoff distances.

### *B. Fast Neutron Detection*

The average counts for stationary standoff detection with the fast neutron detection system are shown in Figure 10; these measurements were taken concurrent with the thermal neutron stationary measurements. Note both the lower count rate from the $^{252}$Cf source as well as the lower background count rate (approximately 20.4 counts/s); based on the measured background rate and a 3σ detection level, the fast detection system would alarm on this source with a 1-s integration at standoff distances of up to approximately 37 m; for a 5-s integration, the system would alarm for standoff distances up to approximately 60 m.

A representative example of the count rate for a drive-by pass (25 m closest approach; 4.7 m/s) with the fast neutron system is shown in Figure 11; the detection results for this system are given in Table 2.

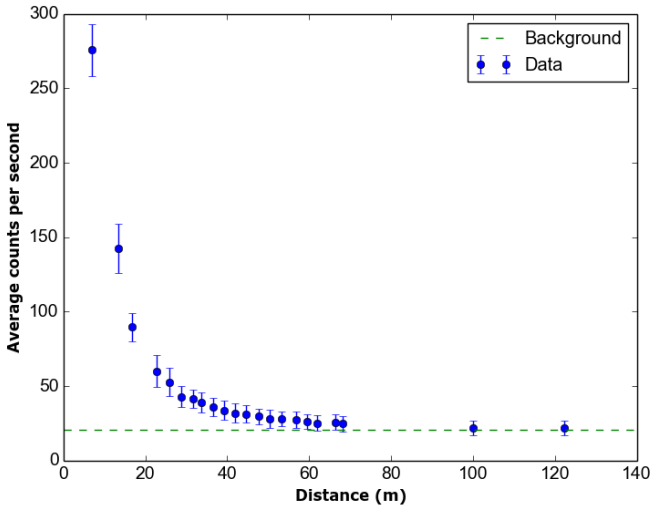


**Figure 10: Average neutron counts per second measured by the fast detection system for stationary measurements. Averages represent approximately 3 min of integration time; error bars represent the actual standard deviations of the data over this integration time.**

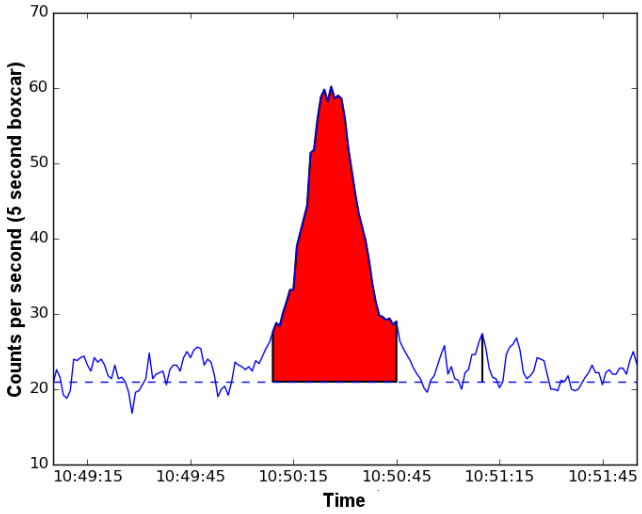


**Figure 11: Representative rate plot for drive-by detection of neutron source (25 m closest approach, 4.7 m/s). The red area indicates the period during which the count rate was greater than 3σ above background.**

**Table 2: Results for mobile detection of neutron source by fast neutron system.**

| Distance (m) | Speed (m/s) | Detection (Y/N) | Boxcar (s) |
|---|---|---|---|
| 17 | 2.9 | Y | 1 |
| 17 | 9.8 | Y | 1 |
| 25 | 2.2 | Y | 1 |
| 25 | 4.7 | Y | 1 |
| 34 | 2.9 | Y | 1 |
| 34 | 4.7 | Y | 1 |
| 34 | 9.4 | Y | 1 |
| 40 | 2.3 | Y | 1 |
| 40 | 4.4 | Y | 1 |
| 44 | 2.8 | Y | 1 |
| 44 | 5.2 | Y | 1 |
| 50 | 2.5 | Y | 1 |
| 50 | 4.8 | Y | 2 |
| 55 | 2.2 | Y | 2 |
| 55 | 4.5 | Y | 2 |
| 60 | 2.3 | Y | 2 |
| 60 | 4.5 | Y | 2 |
| 65 | 2.3 | Y | 2 |
| 65 | 4.5 | Y | 2 |
| 70 | 2.7 | Y | 2 |
| 70 | 4.4 | N | --- |
| 75 | 2.9 | N | --- |
| 75 | 4.3 | N | --- |

## V. DISCUSSION

### *A. On-Water Performance*

Due to the increased hydrogen content of the surrounding media at sea as compared to those on land as well as the relatively large neutron capture cross section of hydrogen, the measured background neutron rate can be expected to decrease for on-water applications; comparison measurements indicate that the background count rate may be on the order of 20% lower on water than on land [4]. As a result, the containerized system may be expected to alarm at greater distances for on-water operations. For example, by assuming a 20% reduction in the background rate for the stationary measurements shown in Figure 8, the standoff distance at which the system would successfully alarm on 1-s integrations increases by approximately 15%.

### *B. Source Localization*

The ability to not only alarm but also localize radioactive sources is extremely valuable. For the fast neutron detection system, this added capability can potentially be realized with the addition of a HPDE coded mask. Previous systems utilizing coded aperture technology on mobile systems to image and localize sources [1, 2] as well as promising results from recent fast neutron coded aperture tests [3] indicate the viability of this approach.

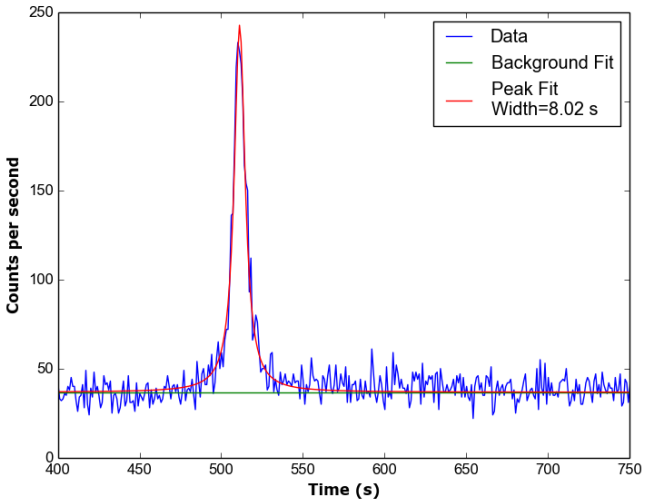


**Figure 12: Lorenztian fit of rate plot for a mobile thermal neutron measurement with a standoff distance of 17 m and a drive-by speed of 4.3 m/s.**

For source localization with the thermal detection system, a different approach is required. For the simple mobile detection operations discussed in this study (straight-line passes) and assuming a standard $r^2$ behavior of the neutron radiation, it can be easily derived that the counts measured by the system should follow a Lorentzian distribution. For a constant speed (which was approximately true for our measurements), the counts $C$ as a function of time $t$ should have the following form:

$$C(t) = A/(t^2 + (w/2)^2) \quad (1)$$

where $A$ is a constant, the peak width $w = 2d/v$, $v$ is the speed of the mobile system, and $d$ is the standoff distance of closest approach. As the source location at closest approach is directly perpendicular to the motion of travel, by recording the GPS location and heading of the mobile system and fitting the distribution of counts to determine the peak width, the location of the source can be determined. An example of such a fit is given in Figure 12 for a 17-m standoff at a drive-by speed of 4.3 m/s. Using the fitted peak width of 8.0 s, the standoff distance of closest approach is calculated to be 17.4 m. More complicated drive-by maneuvers (e.g., curved paths) may require fitting counts in a two-dimensional domain; however, for operations in which simple straight-line passes are viable, this simple peak-fitting procedure may prove valuable.

## VI. Conclusion

The mobile neutron detection system developed at NRL has demonstrated successful detection of fast and thermal neutrons on land at a variety of speeds and standoff distances. For thermal neutron detection, mobile detection was demonstrated for standoff distances up to approximately 100 m; for fast neutron detection, successful detections were shown for distances up to 70 m. On-water performance was predicted by accounting for the expected reduction in the background neutron rate, and a simple source localization algorithm for thermal neutron detection was demonstrated. In addition, further improvements to the fast neutron detection system by the addition of a HDPE coded mask were discussed. This addition as well as actual on-water background and source measurements may provide interesting avenues for future studies.

The containerized neutron detector system described in this work is a fast prototype design and demonstrates the capabilities of a large detection system. Passive detection at large standoff distances requires large-area detection systems; if smaller form factors are desired or required by operational restrictions, the results provided in this work can be scaled to determine the capabilities of such a system. However, such reductions in detection area would be at the cost of standoff capabilities.

## Acknowledgment

The authors of this work gratefully acknowledge the funding from the Chief of Naval Research (CNR). The authors also thank Byron E. Leas (SRA International, Inc.) for his invaluable help during this work.

## References

[1] L. J. Mitchell et al., “Mobile Imaging and Spectroscopic Threat Identification (MISTI): System Overview,” Nuclear Science Symposium Conference Record (NSS/MIC), 2009 IEEE, pp. 110-118, 24 Oct-1 Nov 2009.

[2] A. L. Hutcheson et al., "Maritime Detection of Radiological/Nuclear Threats with Hybrid Imaging System," Technologies for Homeland Security (HST), 2013 IEEE International Conference on, pp. 360-363, 12-14 Nov. 2013.

[3] R. S. Woolf, B. F. Phlips, A. L. Hutcheson, and E. A. Wulf, “Fast Neutron Coded Imager,” Nuclear Instruments and Methods in Physics Research A, Proceedings, in press.

[4] N. N. Voldichev, “Reasons for the Difference between the Fluxes of Electrons and Thermal Neutrons in Secondary Cosmic Rays on Expanses of Glaciers (Water) and Land, Located at the Same Altitude,” Bulletin of the Russian Academy of Sciences: Physics, 2007, vol. 71, no. 7, pp. 1051-1053.